JOURNAL OF OPTIMIZATION THEORY AND APPLICATIONS: Vol. 85, No. 1, pp. 21–57, APRIL 1995

Abort Landing in Windshear: Optimal Control Problem with Third-Order State Constraint and Varied Switching Structure[1]

P. BERKMANN[2] AND H. J. PESCH[3]

Communicated by A. Miele

Abstract. Optimal abort landing trajectories of an aircraft under different windshear-downburst situations are computed and discussed. In order to avoid an airplane crash due to severe winds encountered by the aircraft during the landing approach, the minimum altitude obtained during the abort landing maneuver is to be maximized. This maneuver is mathematically described by a Chebyshev optimal control problem. By a transformation to an optimal control problem of Mayer type, an additional state variable inequality constraint for the altitude has to be taken into account; here, its order is three. Due to this altitude constraint, the optimal trajectories exhibit, depending on the windshear parameters, up to four touch points and also up to one boundary arc at the minimum altitude level. The control variable is the angle of attack time rate which enters the equations of motion linearly; therefore, the Hamiltonian of the problem is nonregular. The switching structures also includes up to three singular subarcs and up to two boundary subarcs of an angle of attack constraint of first order. This structure can be obtained by applying some advanced necessary conditions of optimal control theory in combination with the multiple-shooting method. The optimal solutions exhibit an oscillatory behavior, reaching the minimum altitude level several times. By the optimization, the maximum survival capability can also be determined; this is the maximum wind velocity difference for which recovery from windshear is just possible. The computed optimal trajectories may serve as benchmark trajectories, both for guidance laws that are desirable to approach in actual flight and for

[1]This paper is dedicated to Professor George Leitmann on the occasion of his seventieth birthday.

[2]Graduate Student, Department of Mathematics, Munich University of Technology, Munich, Germany.

[3]Professor of Mathematics, Department of Mathematics, Munich University of Technology, Munich, Germany; presently at Institute of Mathematics, Clausthal University of Technology, Clausthal, Germany.

0022-3239/95/0400-0021$07.50/0

pilot training in flight simulators. They are computed for a realistic windshear model, taking into account the possible presence of updraft/downdraft regions associated with low-altitude windshears accompanied by vortices.

Key Words. Abort landing, windshear-downburst models, Chebyshev optimal control problems, state variable inequality constraints, boundary arcs, touch points, nonregular Hamiltonian, multipoint boundary-value problems, multiple-shooting method.

1. Introduction

Low-altitude windshear must be considered as a contributing factor in many accidents involving large aircraft; see, e.g., Refs. 1 and 2, and the references cited therein. A windshear is usually associated with a downburst, which impacts the surface and causes strong divergent outflows of wind. The divergent headwind–tailwind shear of the downdraft air can easily become strong enough to cause an unmanageable loss of lift to an aircraft penetrating it. A pilot in take-off or landing may be confronted with an increasing headwind which lifts the plane above its intended glideslope. To cope with the headwind, the pilot may take actions to prevent the plane from climbing. These actions are then compounded by performance loss caused by the increased tailwind and downdraft so that the plane may fall below its intended glideslope: A ground impact may then be unavoidable. However, not only the transition from headwind to tailwind is particularly hazardous because of its strong additional acceleration engendered by the windshear, but also strong vertical wind gradients are one of the most dangerous aspects of microbursts; see Ref. 3.

Much effort has therefore gone into modeling and identifying windshear, into numerical computations of safe trajectories for take-off, abort landing, and for penetrating landing, and into the design of controllers to enhance the chances for survival while encountering windshear. Primary among these have been the pioneering studies of Miele; see Refs. 2–19. For a survey, see Ref. 15. Other major contributors to the field of aircraft control are Bryson and Leitmann; see Refs. 20–27. Finally, in order to exemplify the efforts of Russian authors, Refs. 28 and 29 are given in which a game-against-nature approach is employed to deal with the uncertainties due to windshear.

In the present paper, optimal abort landing paths through windshear are computed and investigated. In this respect, the present paper continues the works of Refs. 2 and 11. The optimality criterion to be considered is of minimax type: The minimum altitude obtained during final approach is to be maximized in order to abort the landing maneuver safely. Here, we solve

this Chebyshev optimal control problem directly via a transformation to a third-order state constrained optimal control problem of Mayer type as in Refs. 30 and 31. We do not apply the approximation of the Chebyshev functional by a Bolza functional as in Refs. 2 and 11. Extending the results of Refs. 30 and 31 directly, a new wind model is taken into account which also includes regions with upwinds as they appear in double vortex downbursts. Besides the more general wind model, the survival capability is also computed, i.e., the maximum difference between maximum headwind and maximum tailwind that a windshear can have without engendering an airplane crash. In all those control problem formulations, it is assumed that, upon sensing the aircraft to be in a windshear, the pilot has no opportunity to escape the downburst. For windshear escape problems, see Ref. 32.

From a mathematical point of view, the optimal solutions turn out to exhibit a switching structure of enormous complexity. Since the problem is linear in the control variable, the Hamiltonian is nonregular. Due to this fact and two state constraints involved in the problem, the optimal trajectories consist of multiple subarcs of different kind. There are several bang-bang subarcs, several singular subarcs, and boundary subarcs of both state constraints, as well as several touch points of the minimum altitude level. Therefore, special emphasis is laid on the formulation of the multipoint boundary conditions and jump conditions which are based on the necessary conditions of optimal control theory. The numerical method to be used is the well-known multiple shooting algorithm of Refs. 33 and 34; see also Refs. 35–37. This indirect approach for the solution of the optimal control problems permits one to take advantage of the advanced necessary conditions of Ref. 38. The additional scrutiny allowed by means of these conditions enables the construction of an appropriate switching structure, helps to reject nonoptimal solutions, and thus improves considerably the safety of the candidate optimal trajectory of being really optimal. Those techniques are also explained in detail.

2. Optimal Control Problem

In the following, we summarize briefly the mathematical model as described in Ref. 2, 11, and 30. If the initial altitude is high enough so that it is safer to abort the landing procedure, the flight maneuver can be modeled as a minimax optimal control problem as follows.

2.1. Performance Index. To avoid crashing on the ground, the ground clearance, or in other words the minimal altitude, has to be maximized,

$$\max_{u \in U} \min_{0 \le t \le t_f} h(t); \tag{1}$$

here, U denotes the set of all admissible control variables u, and $[0, t_f]$ is the flight time interval with terminal time t_f not necessarily prescribed. For the numerical computations in Ref. 30, it has been shown to be advantageous to minimize the peak value of the altitude drop instead, that is, the difference between a constant reference altitude h_R and the instantaneous altitude,

$$I[u] := \max_{0 \le t \le t_f} \{h_R - h(t)\} \stackrel{!}{=} \min; \tag{2}$$

here, the reference altitude has to be chosen so as to satisfy

$$h_R \ge h(t), \qquad \forall t \in [0, t_f]. \tag{3}$$

Both performance indices are equivalent. In order to be compatible with Ref. 30, we will retain the latter formulation here, too. This Chebyshev functional can be easily transformed to a Mayer functional by introducing a new variable ζ,

$$\zeta(t) := \max_{0 \le \hat{t} \le t_f} \{h_R - h(\hat{t})\}. \tag{4}$$

Hence, we have the new performance index

$$I[u] = \zeta(t_f) \stackrel{!}{=} \min. \tag{5}$$

Note that ζ is constant. In addition, ζ must satisfy some side conditions which will be specified below.

The optimization is now to be performed subject to several constraints.

2.2. Equations of Motion. Under the assumptions that the aircraft is a particle of constant mass, that the flight takes place in a vertical plane, that Newton's law is valid in an Earth-fixed system, and that the wind flow field is steady, the equations of motion are

$$\dot{x} = V \cos \gamma + W_x, \tag{6a}$$

$$\dot{h} = V \sin \gamma + W_h, \tag{6b}$$

$$\dot{V} = (T/m) \cos(\alpha + \delta) - D/m - g \sin \gamma - (\dot{W}_x \cos \gamma + \dot{W}_h \sin \gamma), \tag{6c}$$

$$\dot{\gamma} = (T/(mV)) \sin(\alpha + \delta) + L/(mV) - (1/V) g \cos \gamma + (1/V)(\dot{W}_x \sin \gamma - \dot{W}_h \cos \gamma), \tag{6d}$$

$$\dot{\alpha} = u; \tag{6e}$$

for the auxiliary variable ζ, we have

$$\dot{\zeta} = 0. \tag{6f}$$

The state variables are the horizontal distance x, altitude h, relative velocity V, relative path inclination γ, and relative angle of attack α. The angle of attack rate u is the control variable here. The models for the aerodynamic forces, i.e., the thrust $T=T(\beta, V)$, drag $D=D(V, \alpha)$, and lift $L=L(V, \alpha)$, can be found in Refs. 2 and 30. In order to be compatible with former results, the power setting β, usually also a control variable, is prescribed as a function of time: Upon sensing the aircraft to be in a windshear, the pilot increases the power setting at a constant time rate until maximum power setting is reached. Then, β is held constant. Note that this fixing of the power setting need not be made, either for the application of the theory or for the application of the numerical method. See the aforementioned references for details of those model functions.

2.3. Wind Models. The influence of the wind is described by the wind velocity components $W_x=W_x(x, h)$ and $W_h=W_h(x, h)$ in the directions of x and h, respectively. The following wind model is used:

$$W_x=kA(x), \tag{7a}$$

$$W_h=k(h/h_*)B(x); \tag{7b}$$

the distribution of the horizontal wind versus the horizontal distance is given by

$$A(x)=\begin{cases} -p+ax^3+bx^4+qx^5, & 0\le x\le x_1, \\ r(x-x_3/2), & x_1\le x\le x_2, \\ p-a(x_3-x)^3-b(x_3-x)^4-q(x_3-x)^5, & x_2\le x\le x_3, \\ p, & x_3\le x; \end{cases} \tag{8a}$$

and the distribution of the vertical wind versus the horizontal distance is given by

$$B(x)=\begin{cases} dx^3+ex^4+sx^5, & 0\le x\le x_1, \\ -51\exp[-c(x-x_3/2)^4], & x_1\le x\le x_2, \\ d(x_3-x)^3+e(x_3-x)^4+s(x_3-x)^5, & x_2\le x\le x_3, \\ 0, & x_3\le x. \end{cases} \tag{8b}$$

Here, the parameter k characterizes the intensity of the windshear/downdraft combination. Its value corresponds to the maximum horizontal wind velocity difference (maximum tailwind minus maximum headwind). By varying the parameters, two different wind models are obtained from Eqs. (8).

Table 1. Parameter values for Wind Model 1.

$x_1 = 500$ ft	$x_2 = 4100$ ft
$x_3 = 4600$ ft	$h_* = 1000$ ft
$a = 6 \times 10^{-8}$ sec^{-1} ft^{-2}	$b = -4 \times 10^{-11}$ sec^{-1} ft^{-3}
$c = -\ln(25/30.6) \times 10^{-12}$ ft^{-4}	$d \approx -8.02881 \times 10^{-8}$ sec^{-1} ft^{-2}
$e \approx 6.28083 \times 10^{-11}$ sec^{-1} ft^{-3}	$k \geq 1$ variable
$p = 50$ ft sec^{-1}	$r = 0.025$ sec^{-1}
$q = 0$ sec^{-1} ft^{-4}	$s = 0$ sec^{-1} ft^{-4}

Table 2. Parameter values for Wind Model 2.

$x_1 = 1300$ ft	$x_2 = 3300$ ft
$x_3 = 4600$ ft	$h_* = 1000$ ft
$a \approx -8.55712 \times 10^{-8}$ sec^{-1} ft^{-2}	$b \approx 1.16943 \times 10^{-10}$ sec^{-1} ft^{-3}
$c = 0.95 \times 10^{-12}$ ft^{-4}	$d \approx 6.45597 \times 10^{-8}$ sec^{-1} ft^{-2}
$e \approx -9.97370 \times 10^{-11}$ sec^{-1} ft^{-3}	$k = 1$
$p = 42$ ft sec^{-1}	$r = 0.04$ sec^{-1}
$q \approx -3.87834 \times 10^{-14}$ sec^{-1} ft^{-4}	$s \approx 3.32076 \times 10^{-14}$ sec^{-1} ft^{-4}

Wind Model 1. This coincides with the wind model used in Ref. 30. It describes a downburst, i.e., a column of fast descending air which spreads out horizontally near the ground. The wind velocity functions W_x and W_h and the wind profile are given in Figs. 1 and 3 of Ref. 30. The values of the parameters are given in Table 1.[4] The parameters a, b, c, d, e are chosen so as to make the functions $A(x)$ and $B(x)$ continuously differentiable at x_1 and x_2 and twice continuously differentiable at x_3. Later, the intensity of the downburst will be increased up to its maximum value k_f which determines the maximum survival capability and which is obtained if the maximinimum of the altitude over ground equals zero. In other words, the maximum survival capability is the critical wind velocity difference ΔW_{xc} for which a crash first occurs.

Wind Model 2. In this model, the parameter c is chosen so as to have, at the border of the downburst, $W_h > 0$, i.e., ascending headwind as well as ascending tailwind. Then, the parameters p and r are determined so that the wind velocity component W_x takes its extremal values approximately at the zeros of W_h. Hence, for both models, the intensity $k = 1$ corresponds to a value of about $\Delta W_x = 100$ ft sec^{-1} for the maximum horizontal wind velocity difference. The additional degree of freedom in the second wind model is used to determine the other parameters so that $A(x)$ and $B(x)$ are twice continuously differentiable. The parameter values are given in Table 2. The

[4]Note that there is a misprint in the formula for $B(x)$, $x_2 \leq x \leq x_3$, in Ref. 30.

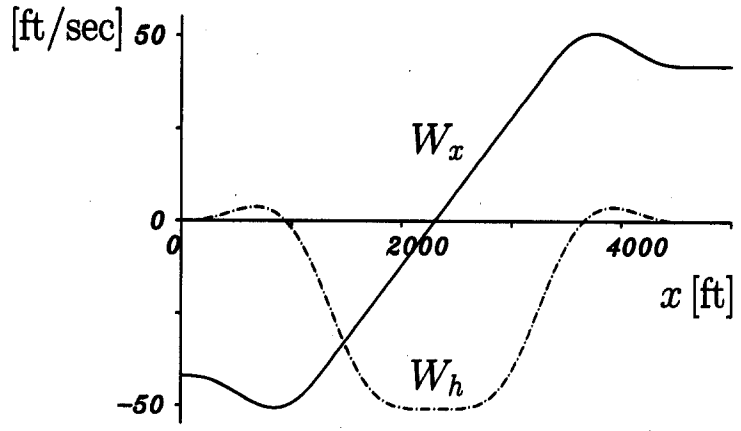

Fig. 1. Wind velocity components for Wind Model 2.

wind velocity components and, for $500\text{ ft} \leq h \leq 600\text{ ft}$, the associated wind flow field are shown in Figs. 1 and 2. This wind profile models the lower half of a double vortex microburst as described, for example, in Refs. 3 and 39. Note that the downburst diameter of this second wind model is smaller than that of the first one.

2.4. Control and State Variable Inequality Constraints. Both the angle of attack and its time derivative are subject to constraints,

$$\alpha \leq \alpha_{\max}, \tag{9}$$

$$u_{\min} \leq u \leq u_{\max}, \qquad u_{\min} = -u_{\max}. \tag{10}$$

Due to the transformation of the Chebyshev functional (2) to the Mayer functional (5), an additional state variable inequality constraint must be taken into account,

$$h_R - h \leq \zeta. \tag{11}$$

2.5. Initial and Terminal Conditions. All state variables (except the auxiliary variable ζ) are prescribed at $t = 0$ based on the assumption of quasi-steady flight prior to the windshear onset. As shown in Ref. 30, optimal trajectories with fixed terminal time $\bar{t}_f$ and γ prescribed at $\bar{t}_f$, due to the

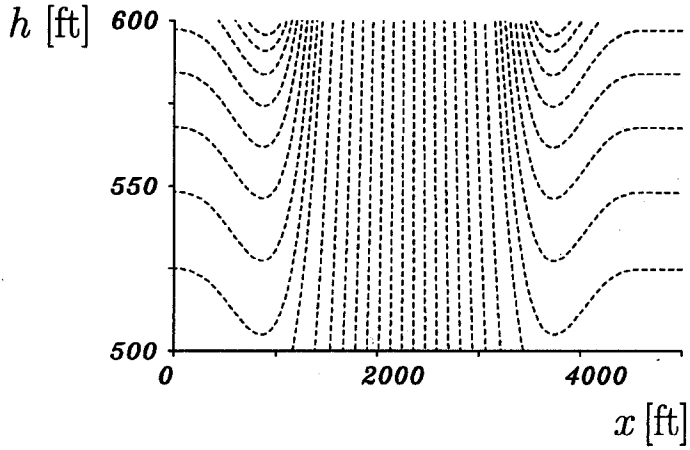

Fig. 2. Wind flow field for Wind Model 2.

steepest climb condition in quasi-steady flight, are optimal trajectories for unspecified terminal time t_f and unspecified γ, too, if $\bar{t}_f$ is large enough. More precisely, $\bar{t}_f$ must be greater than the time at which the altitude h takes its global minimum last.

For the meaning of all other quantities not yet mentioned and for a complete set of all parameters, see Ref. 30.

3. Necessary Conditions

The necessary conditions of optimal control theory for this problem are extensively investigated in Ref. 30, and so we summarize the results only briefly here for the benefit of the reader. To describe the necessary conditions, the notation of Ref. 40 is used; see also Ref. 41 for a summary of practical recipes for the solution of problems of optimal control. The following results provide formulations of the necessary conditions as well-defined multipoint boundary-value problems which also include so-called jump conditions.

Due to the inequality constraints imposed on the problem and because of nonsmooth data in the various model functions, we have to distinguish the following subarcs.

3.1. Bang-Bang and Singular Subarcs. Defining the Hamiltonian on state unconstrained subarcs by

$$H := H^{\text{free}} := \lambda_x \dot{x} + \lambda_h \dot{h} + \lambda_V \dot{V} + \lambda_\gamma \dot{\gamma} + \lambda_a u + \lambda_\zeta \dot{\zeta}, \tag{12}$$

the adjoint vector $\lambda := (\lambda_x, \lambda_h, \lambda_V, \lambda_\gamma, \lambda_\alpha)^\top$ and λ_ζ must solve the system of adjoint differential equations,

$$\dot{\lambda} = -H_y, \qquad y := (x, h, V, \gamma, \alpha)^\top, \tag{13a}$$

$$\dot{\lambda}_\zeta = 0. \tag{13b}$$

By the minimum principle, the optimal control u can be eliminated and substituted in the coupled systems (6) and (13),

$$u = \begin{cases} u_{\max}, & \text{if } \lambda_\alpha < 0, \\ u_{\min}, & \text{if } \lambda_\alpha > 0, \\ u_{\text{sing}}, & \text{if } \lambda_\alpha \equiv 0. \end{cases} \tag{14}$$

In Ref. 30, the complicated expression u_{sing} for the optimal control on singular subarcs can be found, which is obtained by solving $\ddot{\lambda}_\alpha \equiv 0$ for u, while the derivatives are substituted by the right-hand sides of Eqs. (6) and (13). For the problem investigated here, singular subarcs are of order 1. Therefore, the optimal control is either continuously differentiable or discontinuous at junction points between bang-bang and singular subarcs; see Ref. 42. Only the latter case appears in the solutions presented in this paper. Here, it is tacitly assumed that the singular control also satisfies the control variable inequality constraint (10); otherwise, u is bang-bang.

The *a priori* unknown switching points, the switches t_{bang} from $u = u_{\max}$ to $u = u_{\min}$ or vice versa, and the entry and exit points t^s_{entry} and t^s_{exit} of singular subarcs are determined by interior boundary conditions. At the switching points t_{bang}, the switching function λ_α must have isolated zeros,

$$\lambda_\alpha(t_{\text{bang}}) = 0. \tag{15}$$

The switching points t^s_{entry} and t^s_{exit} are determined by one of the pairs of interior boundary conditions (16), (17), or (18),

$$\lambda_\alpha(t^s_{\text{entry}}) = 0, \tag{16a}$$

$$\dot{\lambda}_\alpha(t^s_{\text{entry}}) = 0, \tag{16b}$$

$$\lambda_\alpha(t^s_{\text{exit}}) = 0, \tag{17a}$$

$$\dot{\lambda}_\alpha(t^s_{\text{exit}}) = 0, \tag{17b}$$

$$\lambda_\alpha(t^s_{\text{entry}}) = 0, \tag{18a}$$

$$\lambda_\alpha(t^s_{\text{exit}}) = 0. \tag{18b}$$

In addition, there is a necessary sign condition, the generalized Legendre–Clebsch or Kelley–Kopp–Moyer condition (Ref. 43), which must be satisfied along singular subarcs,

$$(\partial/\partial u)[(d^2/dt^2)H_u] < 0, \qquad t \in [t^s_{\text{entry}}, t^s_{\text{exit}}]. \tag{19}$$

According to the prescribed boundary conditions for the state vector y, the adjoint variables must satisfy the natural boundary conditions. For prescribed terminal path inclination γ at prescribed terminal time $\bar{t}_f$, all components of $\lambda(\bar{t}_f)$ except $\lambda_\gamma(\bar{t}_f)$ must be zero, if no state variable inequality constraint is active at $\bar{t}_f$. Furthermore, there must hold

$$\lambda_\zeta(0) = 0, \tag{20a}$$

$$\lambda_\zeta(\bar{t}_f) = 1. \tag{20b}$$

In total, we have 12 two-point boundary conditions for the 12 unknown state and adjoint functions of the fixed-end-time problem. For terminal time t_f unspecified, see Ref. 30 and Section 4.

3.2. Nonsmooth Data in the Model Functions. Because of nonsmoothness in the model functions for the power setting and the aerodynamic lift coefficient, both the thrust T and lift L have discontinuities in higher derivatives. Therefore, we can conclude that, on singular subarcs, the optimal control variable is discontinuous at points at which $\dot{T}$ or $L_{\alpha\alpha}$ is discontinuous. Moreover, the first derivative of the adjoint variable λ_x is discontinuous at points at which the wind velocity functions are only continuously differentiable. This occurs for the first wind model only.

3.3. Angle of Attack Constrained Subarcs. The state constraint (9) is of order 1. Only boundary subarcs can exist as for regular Hamiltonians. The Hamiltonian is

$$H := H^{\text{free}} + \mu(d/dt)(\alpha - \alpha_{\max}). \tag{21}$$

The right-hand sides of the differential equations for the adjoint variables on a state constrained subarc $[t^\alpha_{\text{entry}}, t^\alpha_{\text{exit}}]$ are identical to those defined on state unconstrained subarcs, since the second term of H does not depend on the state variables explicitly. However, the variable λ_α has a jump discontinuity now, which can be placed either at the entry point or at the exit point of the constrained subarc, e.g.,

$$\lambda_\alpha(t^{\alpha+}_{\text{entry}}) = \lambda_\alpha(t^{\alpha-}_{\text{entry}}) - \sigma_0. \tag{22}$$

For the jump parameter σ_0, a trivial differential equation $\dot{\sigma}_0 = 0$ must be added to Eqs. (6) and (13). The optimal control variable along constrained

subarcs is given by

$$u := u^{\alpha} = 0. \tag{23}$$

The three additional unknowns $t^{\alpha}_{\text{entry}}$, t^{α}_{exit}, and σ_0 are determined by three interior boundary conditions,

$$\alpha(t^{\alpha}_{\text{entry}}) = \alpha_{\max}, \tag{24a}$$

$$\lambda_{\alpha}(t^{\alpha^-}_{\text{entry}}) = 0, \tag{24b}$$

$$\lambda_{\alpha}(t^{\alpha^+}_{\text{exit}}) = 0. \tag{24c}$$

Moreover, the following sign conditions must be satisfied by the Lagrange multiplier μ and the jump parameter σ_0,

$$\mu = \begin{cases} 0, & t \notin]t^{\alpha}_{\text{entry}}, t^{\alpha}_{\text{exit}}[, \\ \geq 0, & t \in]t^{\alpha}_{\text{entry}}, t^{\alpha}_{\text{exit}}[, \end{cases} \tag{25a}$$

$$\dot{\mu} \leq 0, \qquad t \in]t^{\alpha}_{\text{entry}}, t^{\alpha}_{\text{exit}}[, \tag{25b}$$

$$\sigma_0 \geq 0. \tag{25c}$$

3.4. Altitude Constrained Subarcs. The state constraint (11) is of order 3. Contrary to the case of regular Hamiltonians, both boundary arcs and touch points may occur. The Hamiltonian is

$$H := H^{\text{free}} + \bar{\mu}(d^3/dt^3)(h_R - h - \zeta). \tag{26}$$

Touch Points. If the optimal trajectory touches the constraint at a point t^{h}_{touch}, we have two interior boundary conditions for each touch point,

$$h(t^{h}_{\text{touch}}) = h_R - \zeta(t_{\text{touch}}), \tag{27a}$$

$$\dot{h}(t^{h}_{\text{touch}}) = 0, \tag{27b}$$

and also jump conditions,

$$\lambda_h(t^{h^+}_{\text{touch}}) = \lambda_h(t^{h^-}_{\text{touch}}) + \bar{\sigma}, \tag{28a}$$

$$\lambda_{\zeta}(t^{h^+}_{\text{touch}}) = \lambda_{\zeta}(t^{h^-}_{\text{touch}}) + \bar{\sigma}. \tag{28b}$$

The two unknowns t^{h}_{touch} and $\bar{\sigma}$ are determined by the two boundary conditions of Eqs. (27). For the parameter $\bar{\sigma}$, another trivial differential equation must be added to Eqs. (6) and (13). In addition, a sign condition for the parameter $\bar{\sigma}$ must be imposed,

$$\bar{\sigma} \geq 0. \tag{29}$$

Boundary Arcs. On a constrained subarc $[t^h_{\text{entry}}, t^h_{\text{exit}}]$, the optimal control variable is given by

$$u := u^h. \tag{30}$$

The complicated expression for u^h is omitted here; see Ref. 30. It is obtained by solving

$$(d^3/dt^3)(h_R - h - \zeta) \equiv 0$$

for u, where again the derivatives are replaced by the right-hand sides of Eqs. (6) and (13). Here, it is assumed that the boundary control u^h satisfies Eq. (10). The function u^h can have at most one discontinuity caused by the discontinuity of the thrust rate $\dot{T}$, if its discontinuity lies inside the interval $[t^h_{\text{entry}}, t^h_{\text{exit}}]$. Notice that the right-hand sides of the differential equations for the adjoint variables are defined differently on state constrained subarcs, since the second term of H depends also on the state variables.

Five interior boundary conditions at each pair of entry and exit points must be met now,

$$h(t^h_{\text{entry}}) = h_R - \zeta(t^h_{\text{entry}}), \tag{31a}$$

$$\dot{h}(t^h_{\text{entry}}) = 0, \tag{31b}$$

$$\ddot{h}(t^h_{\text{entry}}) = 0, \tag{31c}$$

$$\lambda_\alpha(t^{h^-}_{\text{entry}})[u(t^{h^+}_{\text{entry}}) - u(t^{h^-}_{\text{entry}})] = 0, \tag{31d}$$

$$\lambda_\alpha(t^{h^-}_{\text{exit}})u(t^{h^-}_{\text{exit}}) = \lambda_\alpha(t^{h^+}_{\text{exit}})u(t^{h^+}_{\text{exit}}). \tag{31e}$$

In addition, all of the adjoint variables must satisfy certain jump conditions; e.g., at the entry point,

$$\lambda(t^{h^+}_{\text{entry}}) = \lambda(t^{h^-}_{\text{entry}}) - N_y^\top(t^h_{\text{entry}})(\bar{\sigma}_0, \bar{\sigma}_1, \bar{\sigma}_2)^\top, \tag{32a}$$

$$\lambda_\zeta(t^{h^+}_{\text{entry}}) = \lambda_\zeta(t^{h^-}_{\text{entry}}) + \bar{\sigma}_0, \tag{32b}$$

with

$$N_y = (\partial/\partial y)(h_R - h - \zeta, -\dot{h}, -\ddot{h})^\top$$

and the time derivatives replaced as usual by the right-hand sides of Eqs. (6) and (13). The explicit form of the 5×3 matrix function $N_y^\top$ can also be found in Ref. 30. Again, we have a well-defined set of interior boundary conditions for the five unknowns $t^h_{\text{entry}}, t^h_{\text{exit}}, \bar{\sigma}_0, \bar{\sigma}_1, \bar{\sigma}_2$. For all these jump parameters, trivial differential equations must be added to the system of differential equations.

In addition, some sign conditions must be imposed here, too,

$$\bar{\mu} = \begin{cases} 0, & t \notin]t^h_{\text{entry}}, t^h_{\text{exit}}[, \\ \geq 0, & t \in]t^h_{\text{entry}}, t^h_{\text{exit}}[, \end{cases} \tag{33a}$$

$$\bar{\mu} = -\lambda_\alpha/(\partial/\partial u)[(d^3/dt^3)(h_R - h - \zeta)],$$

$$\dot{\bar{\mu}} \leq 0, \qquad t \in]t^h_{\text{entry}}, t^h_{\text{exit}}[, \tag{33b}$$

$$\ddot{\bar{\mu}} \geq 0, \qquad t \in]t^h_{\text{entry}}, t^h_{\text{exit}}[, \tag{33c}$$

$$\dddot{\bar{\mu}} \leq 0, \qquad t \in]t^h_{\text{entry}}, t^h_{\text{exit}}[, \tag{33d}$$

$$\bar{\sigma}_0 \geq 0, \qquad \bar{\sigma}_1 \geq 0, \qquad \bar{\sigma}_2 \geq 0. \tag{33e}$$

Moreover, the following necessary conditions must also be satisfied at each exit point[5]:

$$\bar{\mu}(t^{h-}_{\text{exit}}) = 0, \tag{34a}$$

$$\dot{\bar{\mu}}(t^{h-}_{\text{exit}}) = 0. \tag{34b}$$

Because of (31e) and the second equation of (33a), Eqs. (34) are equivalent to

$$\lambda_\alpha(t^h_{\text{exit}}) = 0, \tag{35a}$$

$$\dot{\lambda}_\alpha(t^{h-}_{\text{exit}}) = 0. \tag{35b}$$

The first equation can be exchanged for the interior boundary condition (31e), whereas the second equation must be fulfilled additionally. This suggests that a boundary arc might turn into a singular subarc. Since entry and exit points can be interchanged using retrogressive time, Eqs. (35) moreover suggest that an interior boundary arc might be embraced by two singular subarcs. Notice that, according to the minimum principle, a boundary control behaves as a singular control, i.e., there holds $H_u \equiv 0$; see the second equation of (33a).

3.5. Elimination of Auxiliary Variables. In general, some of the variables can be eliminated. If there is a unique minimum (touch point) of the altitude, the auxiliary variables ζ, λ_ζ, $\bar{\sigma}$ can be eliminated from Eqs. (13b), (20), (28b). This yields $\bar{\sigma} = 1$. The trivial differential equations (6f) and (13b) for ζ and λ_ζ, respectively, and that for $\bar{\sigma}$, as well as the two boundary conditions (20) for λ_ζ, the interior boundary condition (27a), and the jump condition (28b), can be dropped. Equation (28a) is a fixed jump condition now.

[5]There is a misprint in the formula after Eq. (38) of Ref. 30: read μ instead of u.

Similarly, the variables $\zeta, \lambda_\zeta, \bar{\sigma}_0$ can be eliminated from Eqs. (6f), (13b), (20), (31a), (32b), if there is a single boundary arc only.

In all other cases, one jump parameter can always be eliminated, since λ_ζ is piecewisely constant with boundary conditions (20). Moreover, the auxiliary variable ζ can be eliminated, too, for example by replacing the boundary conditions (27a) and (31a) by

$$h(t^h_{\text{entry}}) = h(t^h_{\text{touch}}). \tag{36}$$

However, if the minimum altitude, too, is to be computed very precisely, the boundary-value problem should contain

$$\dot{\tilde{\zeta}} = 0, \qquad \tilde{\zeta}(t) := h_{\min} := \min_{0 \le \hat{t} \le t_f} h(\hat{t}), \tag{37a}$$

$$h(t^h_{\text{entry}}) = \tilde{\zeta}(t^h_{\text{entry}}), \qquad h(t^h_{\text{touch}}) = \tilde{\zeta}(t^h_{\text{touch}}). \tag{37b}$$

These equations then replace Eqs. (6f), (27a), (31a).

Furthermore, if the integration is carried through backward, the jump parameter σ_0 can be eliminated. Since $\lambda_\alpha(t^{\alpha+}_{\text{entry}})$ is known then, the jump condition (22) can be performed, because of Eq. (24b), by simply setting

$$\lambda_\alpha(t^{\alpha-}_{\text{entry}}) := 0. \tag{38}$$

In this case, a trivial differential equation for σ_0 must not be included in the system of differential equations. It is true that Eq. (38) coincides with Eq. (24b), but it is a jump condition now and not an interior boundary condition.

Finally, the jump parameter $\bar{\sigma}_2$ can be eliminated, too, if the interior point condition (31d) is satisfied by $\lambda_\alpha(t^{h-}_{\text{entry}}) = 0$. This occurs, if a singular subarc meets the boundary subarc, with respect to the constraint (11), at t^h_{entry}. Notice that this type of junction is just suggested by Eqs. (34) and (35), respectively. In this case, a trivial differential equation for $\bar{\sigma}_2$ must not be included in the system of differential equations, and the interior point condition (31d) must be cancelled. The jump is now performed by setting

$$\lambda_\alpha(t^{h-}_{\text{entry}}) := 0. \tag{39}$$

The integration must also be carried through backward to benefit from this elimination. Again, Eq. (39) has to be considered as a jump condition; it is not an interior boundary condition.

It should be mentioned, however, that it is not useful to apply all of these possible eliminations, since some of the parameters must be computed very precisely, in order to check the necessary sign conditions.

3.6. Multipoint Boundary-Value Problems. In summary, the piecewise-defined differential equations, the two-point boundary conditions, and the

interior boundary conditions form multipoint boundary-value problems for the state variables, adjoint variables, and various jump parameters and switching points. These boundary-value problems depend on the switching structure, i.e., the order of the different subarcs, which has to be presumed and verified *a posteriori*. In addition, some of these variables have to satisfy certain jump conditions. Note that the jump parameters, represented by trivial differential equations, influence the solution via those jump conditions only. Problems of this kind can be solved numerically by an appropriate multiple-shooting method; see, e.g., Refs. 33 and 34. Here, the FORTRAN code BOUNDSCO of Ref. 37 is used; see Ref. 44 for the program and the user manual.

All of the above-mentioned sign conditions and also the exit conditions (34) for $\bar{\mu}$, which for the greater part go back to Ref. 38 (see also Theorem 3.1 in Ref. 30 and Ref. 45), are of utmost importance for the rejection of nonoptimal solutions. In addition, changes of the switching structure are indicated by means of these conditions, as will be seen in the following sections. Note that these conditions are not part of the boundary-value problem itself, but they must be verified together with the switching structure afterward.

4. Optimal Trajectories for Wind Model 1

Starting point for the computations is the optimal control problem for the first wind model with the windshear intensity $k=1$, a candidate optimal solution of which has been published in Ref. 31. The associated switching structure was found to be

$$u_{\min}|u_{\text{sing}}|u^h|u_{\max}|u_{\text{sing}}|u^a|t^h_{\text{touch}}|u^a|u_{\min}. \tag{40}$$

The different subarcs are separated by vertical dashes, where touch points are considered as subarcs of zero length.

First, the survival capability is to be computed. In order to compute the maximum difference between maximum headwind and maximum tailwind that a windshear can have without engendering an airplane crash during the abort landing, the intensity parameter k is increased until a critical value k_f is found, such that $h_{\min}=0$. Hence, this critical value k_f is defined by

$$\dot{k}=0, \tag{41a}$$

$$\tilde{\zeta}(\bar{t}_f)=0. \tag{41b}$$

The dimension of the boundary-value problem must then be increased by 1. Numerically, the solution can be obtained via a homotopy by which the parameter k is increased stepwise, here with a stepsize $\Delta k \approx 0.02$.

Right at the beginning of the homotopy, however, the solution due to the above switching structure (40) does not satisfy sufficiently accurately the necessary exit condition (34b) for the Lagrange multiplier $\bar{\mu}$ or the equivalent Eq. (35b), respectively. Notice that the boundary arc is here not embraced by two singular subarcs, as was pointed out in Section 3. Hence, another singular subarc must be inserted into the above switching structure. Additionally, a second touch point appears. The new switching structure is now

$$u_{\min}|u_{\text{sing}}|u^h|u_{\text{sing}}|u_{\max}|t^h_{\text{touch},1}|u_{\max}|u_{\text{sing}}|u^a|t^h_{\text{touch},2}|u^a|u_{\min}. \tag{42}$$

The candidate optimal solution from Ref. 31 can also be improved by means of this switching structure. The value of $\dot{\bar{\mu}}(t^{h-}_{\text{exit}})$ then increases from about -0.8×10^{-2} to about -0.8×10^{-13}, resulting in an increase of the minimum altitude from $h_{\min} = 502.1562783$ ft to $h_{\min} = 502.1562810$ ft. Of course, the diminutiveness of 3×10^{-6} ft in the increase of the performance index is of no practical importance. However, it underscores the remarkable accuracy which can be obtained by the multiple-shooting method. Figure 3 shows the altitude history, and the enlargement shows the second touch point released at the end of the boundary arc. The optimal trajectory includes three branches: a descending flight branch, followed by a slightly oscillating, nearly horizontal flight branch, followed by an ascending flight branch after the aircraft has passed through the shear region. This corresponds to the experience that an initial climb will be penalized by a stall at a later time. Notice that the last point on the minimum altitude level is just at $t = t_f$, with

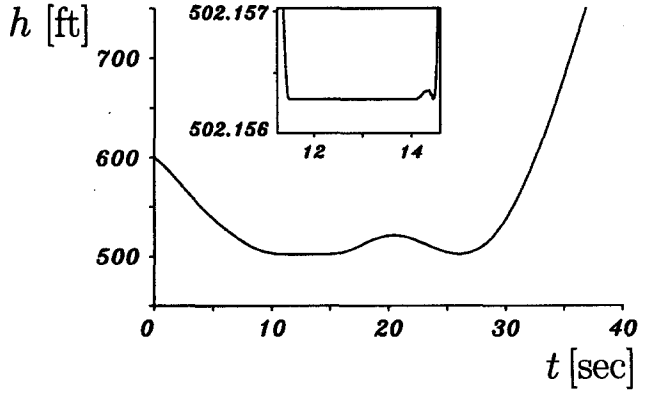

Fig. 3. Altitude versus time for Wind Model 1, $k = 1$, one boundary arc and two touch points.

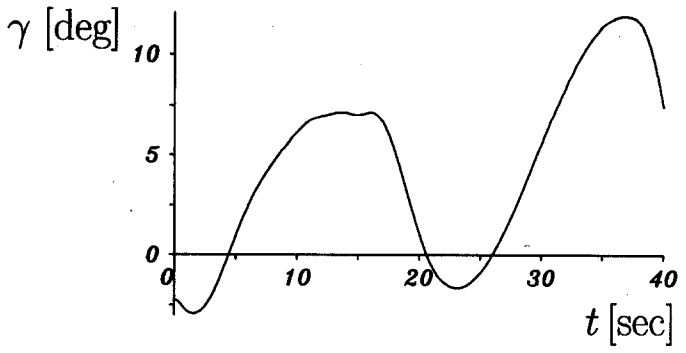

Fig. 4. Path inclination versus time for Wind Model 1, $k=1$.

t_f being the terminal time of the open endtime problem: Since the optimal trajectory for this problem ends on a boundary subarc of the angle of attack constraint, thus $\alpha(t_f)=\alpha_{\max}$, $\lambda_\alpha(t_f)$ must not necessarily vanish. Because $\dot{h}(f)=\dot{\alpha}(t_f)=0$, the transversality condition for free terminal time is however, satisfied,

$$H|_{t_f}=\lambda_h(t_f)\dot{h}(t_f)+\lambda_\alpha(t_f)\dot{\alpha}(t_f)=0. \tag{43}$$

In Figs. 4–7, the histories of the path inclination, angle of attack, switching function λ_α, and corresponding angle of attack rate u are presented. The state variables of the suboptimal solution given in Ref. 31 coincide, within drawing accuracy, with the results presented here. Along an optimal trajectory, points near the minimum velocity are reached twice, at the end of the shear and near $t=\bar{t}_f$; see Fig. 37 of Ref. 31. At the beginning, the airspeed

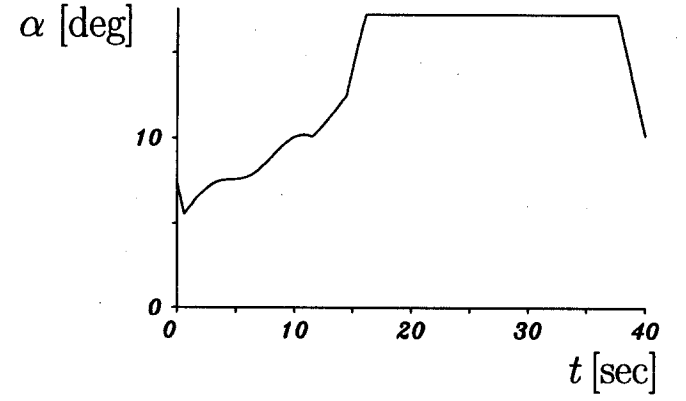

Fig. 5. Angle of attack versus time for Wind Model 1, $k=1$, one boundary subarc.

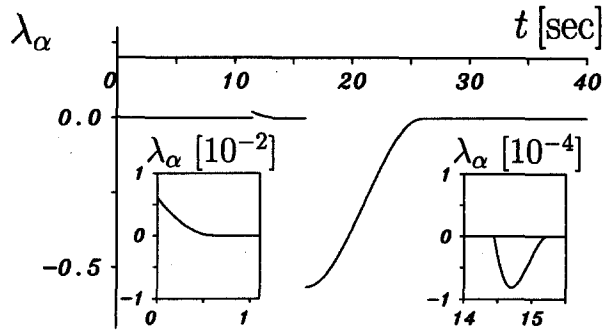

Fig. 6. Adjoint variable λ_α versus time for Wind Model 1, $k=1$.

is increased and the aircraft is placed in a region of lower downdraft velocity to enhance the chances of recovery from the microburst. The pilot should trade altitude for airspeed. A comparison of Figs. 6 and 7 brings much insight into the important role of the switching function λ_α for the choice of the optimal angle of attack rate u. Initially, the angle of attack must be reduced, which will be seen later to depend very sensitively on the windshear parameters; compare Figs. 5–7, in particular the first detail of Fig. 6. Despite the special scaling for the switching function in the second detail of this figure, it cannot be seen clearly that $\dot{\lambda}_\alpha$, too, vanishes at the exit point of the second singular subarc as well as at the entry point of the third singular subarc, as is dictated by necessary conditions. The detail of Fig. 7 shows the discontinuous junction between the boundary arc with respect to the altitude constraint and the subsequent second singular subarc. The control u is also discontinuous inside the first singular subarc, due to the discontinuity of the thrust rate $\dot{T}$. This discontinuity, however, is below drawing accuracy; compare the similar situation in Fig. 13.

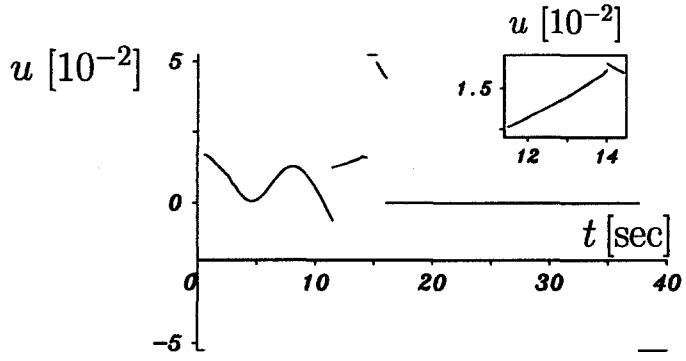

Fig. 7. Angle of attack rate u (control) versus time for Wind Model 1, $k=1$.

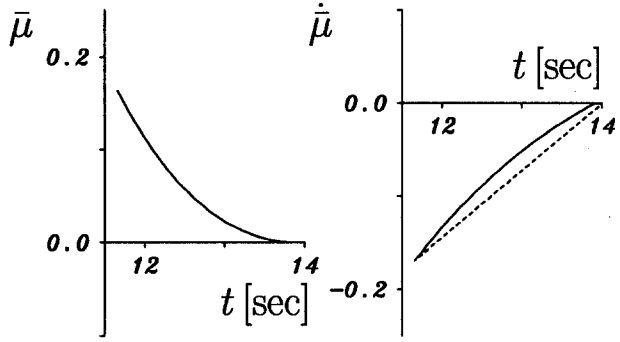

Fig. 8. Lagrange multiplier $\bar{\mu}$ and $\dot{\bar{\mu}}$ versus time for Wind Model 1, $k=1$.

For a check of the important necessary conditions (33a–d) and (34), see Fig. 8. Needless to say, all other sign conditions mentioned in the present paper are also satisfied, and this for progressive as well as retrogressive time; compare Ref. 30.

Table 3 gives approximations for the various switching points, and the equations of the 15 interior boundary conditions for the 9 switching points and 6 parameters: ζ (or $\tilde{\zeta}$, respectively), $\bar{\sigma}^{(1)}$, $\bar{\sigma}^{(2)}$ (for two touch points), $\bar{\sigma}_1$, $\bar{\sigma}_2$ [$\bar{\sigma}_0 = 1 - \bar{\sigma}^{(1)} - \bar{\sigma}^{(2)}$], and σ_0. The number of interior boundary conditions to be fulfilled at the various switching points is given in square brackets. The jump conditions are also listed. Note that the formulation of the multipoint boundary-value problem is generally not unique; see, e.g., Eqs. (16)–(18). Equation (18) usually leads to a better convergence of the multiple-shooting method.

In the course of the homotopy toward maximum windshear intensity, the switching structure has to be adjusted twice. Firstly, the boundary subarc due to the third-order state constraint shrinks to a third touch point. Secondly, the singular control violates the lower bound of Eq. (10). Hence, another bang-bang subarc must be inserted. Furthermore, additional discontinuities in the approximation of the aerodynamic lift coefficient cause two additional discontinuities of the singular control.

We end up with the following switching structure

$$u_{\min}|u_{\text{sing}}|u_{\min}|t^h_{\text{touch},1}|u_{\min}|u_{\text{sing}}|u_{\max}|t^h_{\text{touch},2}|u_{\max}|u_{\text{sing}}|u^a|t^h_{\text{touch},3}|u^a|u_{\min}. \quad (44)$$

The maximum value of k according to Eqs. (41) is $k=k_f \approx 2.00366$ corresponding to a maximum survival capability of about $\Delta W_{xc}=200$ ft/sec, which is about the size of the largest values obtained from real data (compare Ref. 46) and about 5% higher than the value given in Ref. 6. The optimal trajectory, showing three touch points of the third-order state constraint, is

Table 3. Interior conditions for Wind Model 1 ($k=1$).

Switching points	t (sec)	Interior boundary conditions	Jump conditions
$t^s_{\text{entry},1}$	0.61		
$t^h_{\text{entry}}=t^s_{\text{exit},1}$	11.51	Eqs. (31a–c) [3][a] Eqs. (17) [2][c]	Eqs. (32a)[c]
$t^s_{\text{entry},2}=t^h_{\text{exit}}$	14.01	Eq. (31e) [1][d]	
$t^s_{\text{exit},2}$	14.43	Eq. (18b) [1]	
$t^h_{\text{touch},1}$	14.46	Eqs. (27) [2][a]	Eq. (28a)
$t^s_{\text{entry},3}$	15.22		
$t^a_{\text{entry}}=t^s_{\text{exit},3}$	16.09	Eq. (24a) [1] Eqs. (17) [2][b]	Eq. (22)[b]
$t^h_{\text{touch},2}$	26.00	Eqs. (27) [2][a,e]	Eq. (28a)
t^a_{exit}	37.65	Eq. (24c) [1]	

[a] If $\tilde{\zeta}=h_{\min}$ is to be used as parameter, Eqs. (27a) and (31a) have to be replaced by Eqs. (37b).

[b] If σ_0 is to be eliminated, Eq. (22) has to be replaced by Eq. (38). In this case, Eq. (17a) must be cancelled and the integration must be performed in a backward manner.

[c] Here, $\bar{\sigma}_2$ can be eliminated from the fifth component of Eq. (32a). For that, Eq. (17a) has to be cancelled and the fifth component of Eq. (32a) has to be replaced by (39). In the other components of Eq. (32a), $\bar{\sigma}_2$ has to be substituted. The integration must also be performed backward here.

[d] Alternatively, Eq. (35a) [1].

[e] Here, the transversality conditions for the terminal time and the terminal flight path angle, both unspecified, are additionally satisfied.

given in Figs. 9–14. Basically, the optimal trajectory reaches the minimum altitude level $h_{\min}=0$ twice, and the velocity drops to about 160 ft/sec at the end of the shear region. The figures for the path inclination and angle of attack show clearly the advantage of a descending flight branch for the recovery maneuver. The reduction of the angle of attack turns out to be the more distinct the more severe the shear is. Notice that the singular control subarc has three discontinuities, one caused by the discontinuity of $\dot{T}$ at $t\approx 3.09$ sec (see the detail in Fig. 13) and two caused by the discontinuity of $L_{\alpha\alpha}$ at $\alpha=\alpha_{**}:=12$ deg (before and after $t=10$ sec; see Figs. 13 and 14). The details in Fig. 12 show the switching function λ_α along the second and third bang-bang subarc, both encircled by singular subarcs.

In summary, one has obtained the following result: For Wind Model 1, there exists no abort landing trajectory through the microburst if the intensity factor exceeds $k=k_f$. Only penetrating landing might then be possible.

Table 4 lists the interior point conditions and jump conditions for Wind Model 1 with $k=k_f$. The unknowns to be determined are 10 switching points

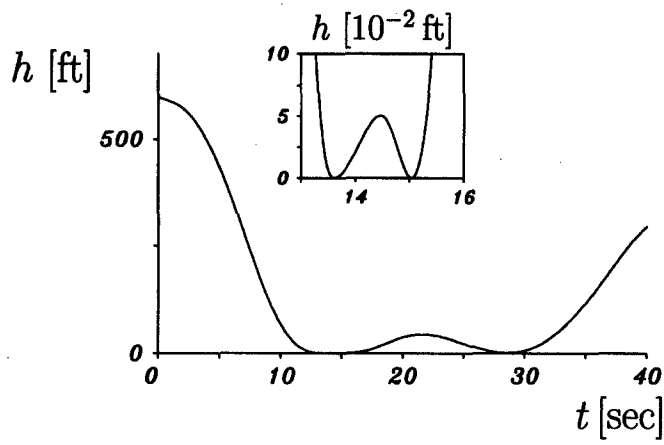

Fig. 9. Altitude versus time for Wind Model 1, $k=k_f$, three touch points.

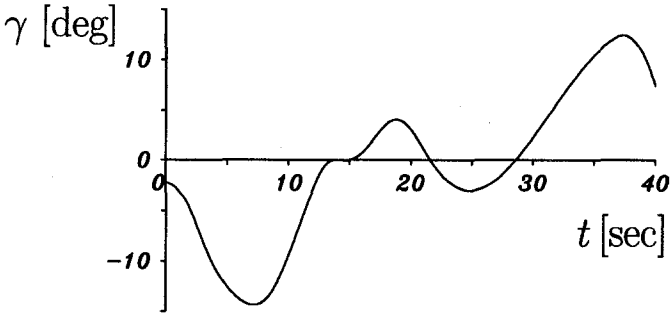

Fig. 10. Path inclination versus time for Wind Model 1, $k=k_f$.

and 4 parameters: ζ (or $\tilde{\zeta}$, respectively), $\bar{\sigma}^{(1)}$, $\bar{\sigma}^{(2)}$ [for three touch points, $\bar{\sigma}^{(3)}=1-\bar{\sigma}^{(1)}-\bar{\sigma}^{(2)}$], and σ_0.

5. Optimal Trajectories for Wind Model 2

The starting point for the computations is the optimal solution for the first wind model with intensity factor $k=1$ now fixed. By means of homotopies with respect to the four parameters x_1 (where $x_2:=x_3-x_1$), c, r, p, the optimal solution for the second wind model can be obtained. During these computations, the solutions of the various multipoint boundary-value problems must be carefully checked for changes of the switching structure. In the case of changing switching structures, the control laws, eventually the

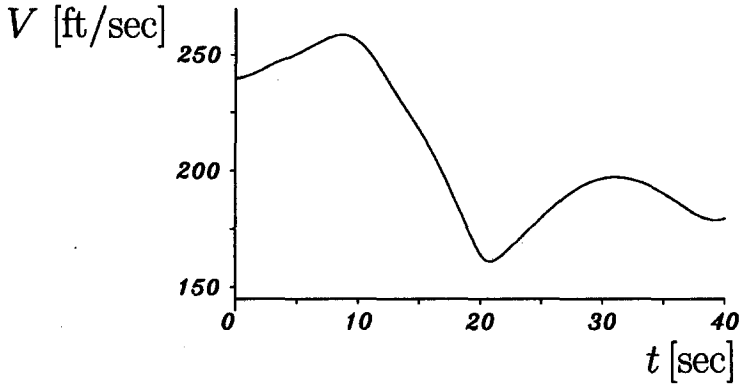

Fig. 11. Velocity versus time for Wind Model 1, $k=k_f$.

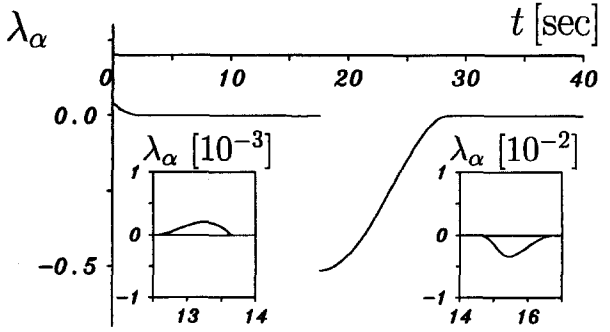

Fig. 12. Adjoint variable λ_α versus time for Wind Model 1, $k=k_f$.

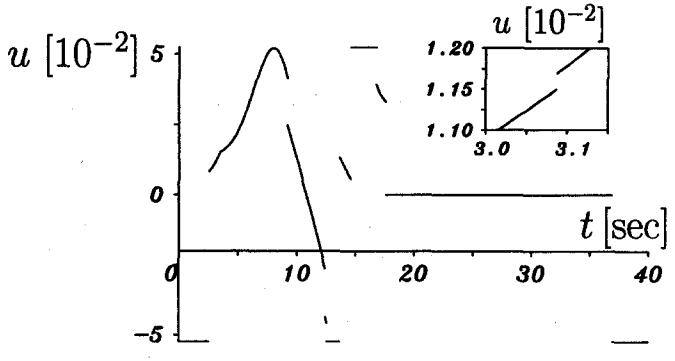

Fig. 13. Angle of attack rate u (control) versus time for Wind Model 1, $k=k_f$.

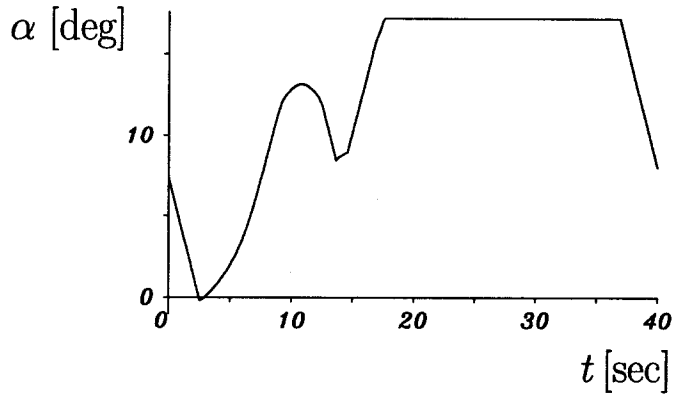

Fig. 14. Angle of attack versus time for Wind Model 1, $k=k_f$, one boundary subarc.

right-hand sides of the adjoint differential equations, and the interior boundary conditions must be appropriately adjusted. These changes of the switching structure are indicated, for example, by the following events:

(i) If the sign of the switching function does not match the control law (14), the bang-bang/singular structure must be appropriately adjusted.

(ii) If the singular control u_{sing} violates the control constraint (10), an appropriate bang-bang subarc must be introduced. According to Ref.

Table 4. Interior conditions for Wind Model 1 ($k=k_f$).

Switching points	t (sec)	Interior boundary conditions	Jump conditions
$t^s_{\text{entry},1}$	2.52	Eq. (18a) [1]	
$t^s_{\text{exit},1}$	12.55	Eq. (18b) [1]	
$t^h_{\text{touch},1}$	13.61	Eqs. (27) [2][a]	Eq. (28a)
$t^s_{\text{entry},2}$	13.65	Eq. (18a) [1]	
$t^s_{\text{exit},2}$	14.59	Eq. (18b) [1]	
$t^h_{\text{touch},2}$	15.04	Eqs. (27) [2][a]	Eq. (28a)
$t^s_{\text{entry},3}$	16.77	Eq. (18a) [1]	
$t^a_{\text{entry}}=t^s_{\text{exit},3}$	17.62	Eq. (24a) [1]	Eq. (22)[b]
		Eq. (24b) [1][b]	
$t^h_{\text{touch},3}$	28.58	Eqs. (27) [2][a,c]	Eq. (28a)
t^a_{exit}	36.92	Eq. (24c) [1]	

[a] If $\tilde{\zeta}$ is used as parameter, Eq. (27a) has to be replaced by the second equation of Eqs. (37b).

[b] If σ_0 is to be eliminated, Eq. (22) has to be replaced by Eq. (38). In this case, Eq. (24b) must be cancelled and the integration must be performed in a backward manner.

[c] Here, the transversality conditions for the terminal time and the terminal flight path angle, both unspecified, are additionally satisfied.

42, the junction is either discontinuous or continuously differentiable. Here, only discontinuous junctions have appeared.

(iii) A violation of the sign conditions (25) in the interior of an angle of attack constrained subarc indicates that this subarc breaks up into two subarcs separated by two bang-bang subarcs.

(iv) A local minimum of the altitude with $h < \zeta$ (or $h_R - h > \zeta$, respectively) indicates the appearance of either another touch point or another boundary subarc. In the present problem, a touch point always precedes a boundary subarc in case the constraint (11) becomes active, and vice versa in case Eq. (11) becomes inactive.

(v) A shrinking altitude-constrained subarc indicates its transition to a touch point or possibly its complete disappearance. This can also be seen from the sign conditions (33).

(vi) If the condition $\ddot{h}(t^h_{\text{touch}}) \geq 0$ is violated, either the touch point splits into two touch points or changes into a boundary subarc.

(vii) One of two touch points disappears, since the associated jump parameter becomes negative.

(viii) If the jump parameters in Eqs. (32) and (33) decrease toward zero, the boundary subarc may turn into one touch point.

Table 5 gives a survey of the homotopies and different switching structures that have occurred. It should be mentioned that a favorable ordering can reduce both human labor and computing time considerably. However, the homotopies have not been optimized in this respect here. Figures 15–20 show some of the intermediate results concerning the altitude histories. The optimal trajectories basically stay three or four times near the level of minimum ground clearance, which varies roughly between 530 ft and 590 ft. In this way, a pilot can benefit from the upwinds if controlling close to the optimum.

Figures 21–26 show the optimal trajectories for Wind Model 2. The considerable increase of the altitude just before the end of the shear region (Fig. 21) corresponds to the velocity drop to about 160 ft/sec (Fig. 23), immediately followed by the last point of closest approach to the surface. Notice also the change of the sign of the angle of attack rate at the beginning, both during the homotopies (Table 5) and for Wind Model 2 (Figs. 25 and 26). This indicates a considerable sensitivity with respect to the windshear parameters. Again, the necessary conditions (16)–(18) are satisfied; however, they cannot all be resolved by the details of Fig. 24. The detail of Fig. 25 shows the discontinuous junction between the second tiny bang-bang subarc and the first singular subarc, which turns out to be typical for first-order singular subarcs, at least for the problems investigated here. Also, the junctions between the boundary subarc with respect to the altitude constraint

Table 5. Change of the switching structure during homotopies.

Parameter[a]	Switching structure[b]								Index[c]
$x_1 = 500$	$u_{\min}$	u_{sing}	u^h	u_{sing}	$u_{\max}\|\text{TP}\|u_{\max}$	u_{sing}	$u^\alpha\|\text{TP}\|u^\alpha$	$u_{\min}$	Eq. (42)
$x_1 = 1300$	unchanged								
$c \approx 0.2021$	see $x_1 = 1300$								
$c = 0.4525$	$u_{\min}$	$u_{\text{sing}}\|\text{TP}\|u_{\text{sing}}$	u^h	u_{sing}	$u_{\max}\|\text{TP}\|u_{\max}$		$u^\alpha\|\text{TP}\|u^\alpha$	$u_{\min}$	(i), (iv)
$c = 0.7$	$u_{\max}$	$u_{\text{sing}}\|\text{TP}\|u_{\text{sing}}$	u^h	u_{sing}	$u_{\max}\|\text{TP}\|u_{\max}$		$u^\alpha\|\text{TP}\|u^\alpha$	$u_{\min}$	(i)
$c = 0.8$	$u_{\max}$		$u_{\text{sing}}\|\text{TP}\|u_{\text{sing}}\|\text{TP}\|u_{\text{sing}}$		$u_{\max}\|\text{TP}\|u_{\max}$		$u^\alpha\|\text{TP}\|u^\alpha$	$u_{\min}$	(v)
$c = 0.9$	$u_{\max}$	u_{sing}	u^h	$u_{\text{sing}}\|\text{TP}\|u_{\text{sing}}$	$u_{\max}\|\text{TP}\|u_{\max}$		$u^\alpha\|\text{TP}\|u^\alpha$	$u_{\min}$	(vi)
$c = 0.95$	$u_{\max}$	u_{sing}	u^h	u_{sing}	$u_{\max}\|\text{TP}\|u_{\max}$		$u^\alpha\|\text{TP}\|u^\alpha$	$u_{\min}$	(vii)
$r = 0.025$	see $c = 0.95$								
$r = 0.026$	$u_{\max}$		$u_{\text{sing}}\|\text{TP}\|u_{\text{sing}}$		$u_{\max}\|\text{TP}\|u_{\max}$		$u^\alpha\|\text{TP}\|u^\alpha$	$u_{\min}$	(viii)
$r = 0.029$	$u_{\max}$		$u_{\text{sing}}\|\text{TP}\|u_{\text{sing}}$		$u_{\max}\|\text{TP}\|u_{\max}$	u_{sing}	$u^\alpha\|\text{TP}\|u^\alpha$	$u_{\min}$	(i)
$r = 0.033$	$u_{\min}$		$u_{\text{sing}}\|\text{TP}\|u_{\text{sing}}$		$u_{\max}\|\text{TP}\|u_{\max}$	u_{sing}	$u^\alpha\|\text{TP}\|u^\alpha$	$u_{\min}$	(i)
$r = 0.039$	$u_{\min}$		$u_{\text{sing}}\|\text{TP}\|u_{\text{sing}}$		$u_{\max}\|\text{TP}\|u_{\max}$	u_{sing}	u^α	TP $u_{\min}$ $u_{\max}$ u^α	(iii)
$r = 0.04$	see $r = 0.039$								
$p = 0.05$	see $r = 0.039$								
$p = 0.047$	$u_{\max}$		$u_{\text{sing}}\|\text{TP}\|u_{\text{sing}}$		$u_{\max}\|\text{TP}\|u_{\max}$	u_{sing}	u^α	TP $u_{\min}$ $u_{\max}$ u^α	(i)
$p = 0.044$	$u_{\max}$	u_{sing}	u^h	u_{sing}	$u_{\max}\|\text{TP}\|u_{\max}$	u_{sing}	u^α	TP $u_{\min}$ $u_{\max}$ u^α	(vi)
$p = 0.042$	$u_{\max}$ $u_{\min}$	u_{sing}	u^h	u_{sing}	$u_{\max}\|\text{TP}\|u_{\max}$	u_{sing}	u^α	TP $u_{\min}$ $u_{\max}$ u^α	(ii)

[a] Homotopy parameters near which or starting at which a change of the switching structure occurs.
[b] Notation: TP stands for a touch point.
[c] Index referring to the list of events by which changes of the switching structure are indicated.

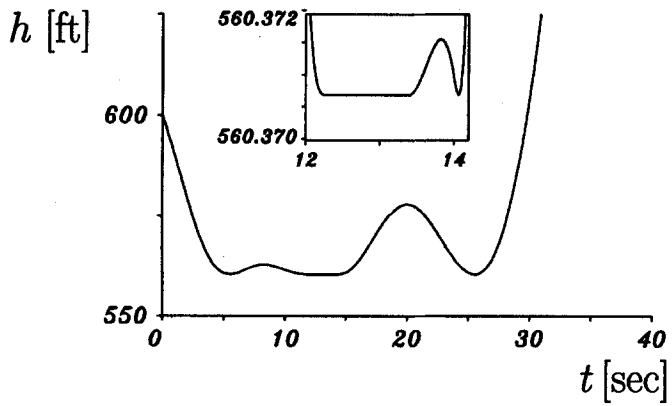

Fig. 15. Altitude versus time, one boundary arc and three touch points, $c=0.60$.

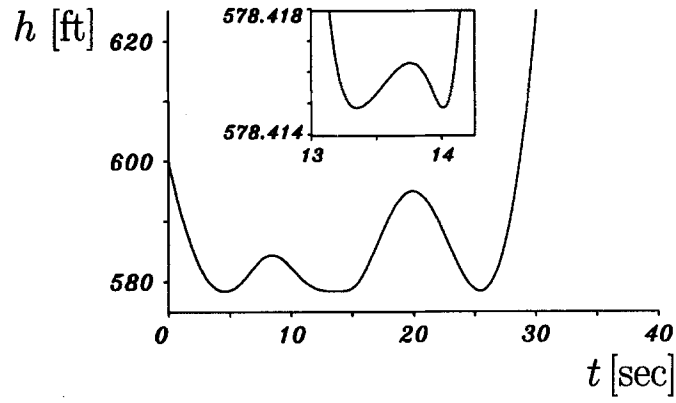

Fig. 16. Altitude versus time, four touch points, $c=0.80$.

and the two adjacent singular subarcs are discontinuous. Additionally, there is a discontinuity of the control inside that boundary subarc, which is caused by the nonsmooth approximation of the power setting. In Fig. 27, the important Lagrange multiplier $\bar{\mu}$ is shown, indicating that the additional necessary conditions (33) and (34) are also satisfied.

Finally, Table 6 gives the 18 (!) interior boundary conditions and the jump conditions for the formulation of the multipoint boundary-value problem. There are 11 switching points and 7 parameters to be determined: ζ (or $\tilde{\zeta}$, respectively), $\bar{\sigma}^{(1)}$, $\bar{\sigma}^{(2)}$ (for two touch points), $\bar{\sigma}_1$, $\bar{\sigma}_2$ [$\bar{\sigma}_0 = 1 - \bar{\sigma}^{(1)} - \bar{\sigma}^{(2)}$], $\sigma_0^{(1)}$, $\sigma_0^{(2)}$ [for two subarcs due to the constraint (9)]. Recall that, at the last touch point, the natural boundary condition (43) for unprescribed terminal

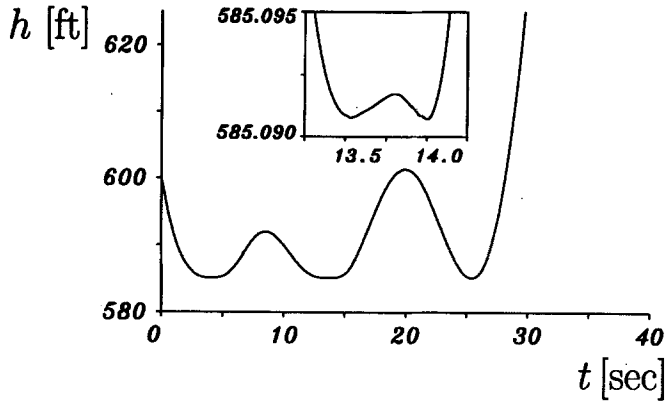

Fig. 17. Altitude versus time, one boundary arc and three touch points, $c=0.90$.

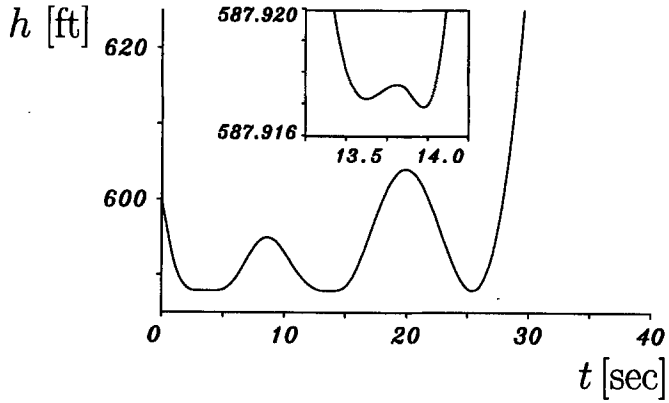

Fig. 18. Altitude versus time, one boundary arc and two touch points, $c=0.95$.

time t_f is satisfied, too. Hence, the optimal trajectories for unspecified terminal time have been simultaneously obtained.

6. Conclusions

Maximum ground clearance abort landing trajectories for an airplane encountering windshear have been computed by means of the necessary conditions of optimality for the underlying Chebyshev optimal control problem and by means of the multiple-shooting method for the solution of the resulting multipoint boundary-value problems. Two different wind profiles

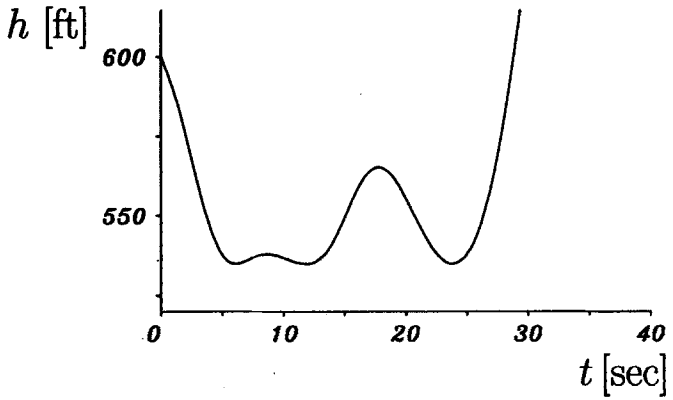

Fig. 19. Altitude versus time, three touch points, $r = 0.04$.

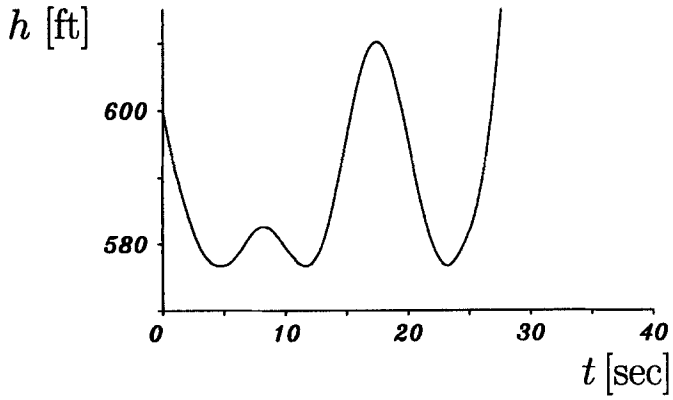

Fig. 20. Altitude versus time, three touch points, $p = 0.044$.

have been employed and their influence on the optimal trajectories has been investigated. The numerical results show a considerable sensitivity of the optimal trajectories with respect to these wind profiles. If a windshear includes regions with upwinds, the altitude drop during the abort landing maneuver is much less than in a plain downburst of the same maximum wind velocity difference. However, the level of closest approach to the ground is reached up to four times depending on the shear models investigated here. To take advantage of the upwinds, a high price has to be paid in the form of a very complicated history of the angle of attack rate, which is the control function here. In addition, the maximum survival capability has been computed to be 200 ft/sec for a certain microburst model, which is of about the

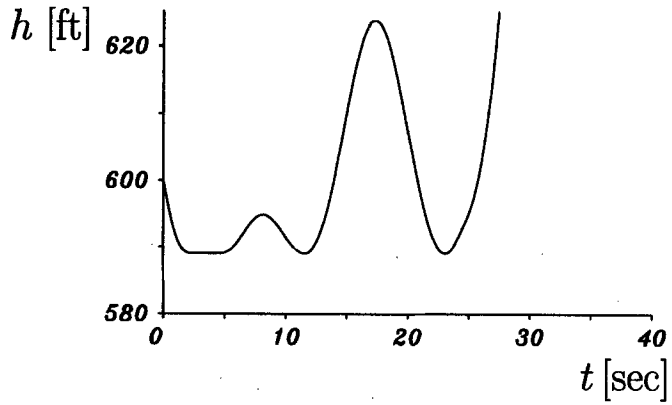

Fig. 21. Altitude versus time for Wind Model 2, one boundary arc and two touch points.

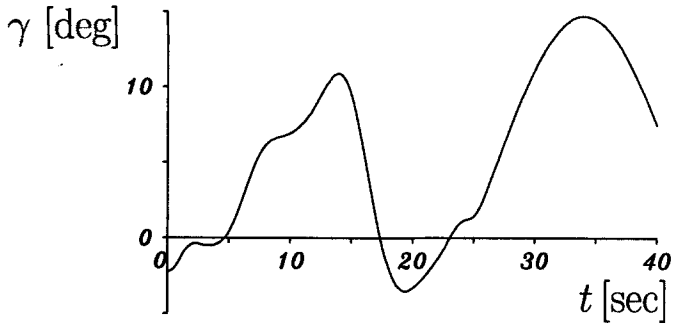

Fig. 22. Path inclination versus time for Wind Model 2.

size of the largest values obtained from real data. The different windshear/downburst combinations and their associated optimal abort landing flight paths over ground are compared in Figs. 28–30.

The problem seems to be also of special mathematical interest. Since the Hamiltonian is nonregular, theoretical results about the existence of boundary arcs and touch points generally do not apply. Moreover, the theorems developed in Ref. 38 for optimal control problems with controls appearing linearly cannot be applied either, since the orders of the state constraints and singular subarcs do not match the assumptions of those theorems. There is a lack of appropriate theoretical results about the existence of boundary arcs and/or touch points for nonregular Hamiltonian.

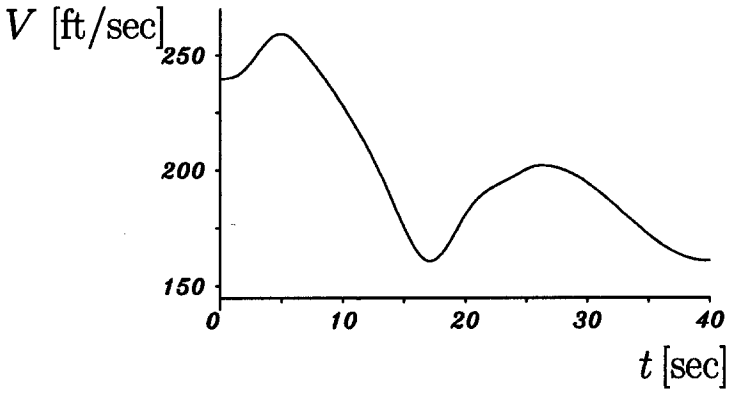

Fig. 23. Velocity versus time for Wind Model 2.

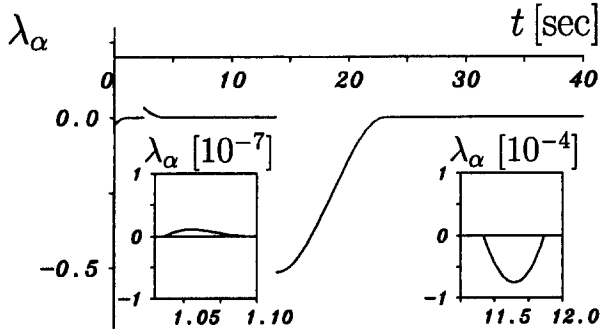

Fig. 24. Adjoint variable λ_α versus time for Wind Model 2.

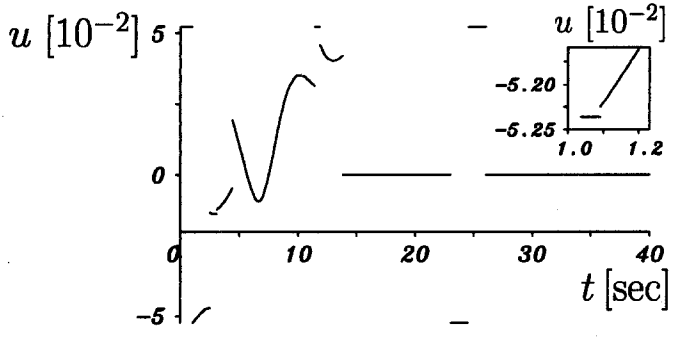

Fig. 25. Angle of attack rate u (control) versus time for Wind Model 2.

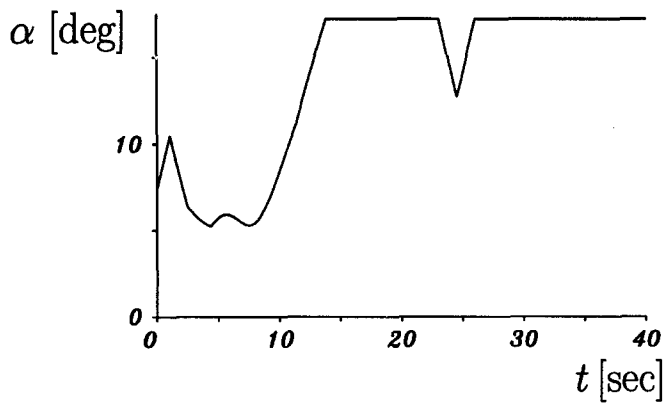

Fig. 26. Angle of attack versus time for Wind Model 2, two boundary subarcs.

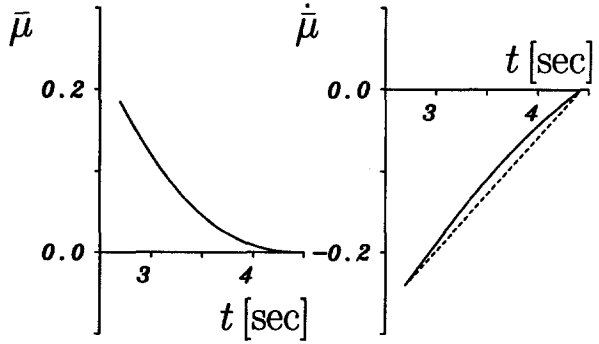

Fig. 27. Adjoint variable $\bar{\mu}$ and $\dot{\bar{\mu}}$ versus time for Wind Model 2.

The computed (candidate) optimal trajectories exhibit, depending on the windshear parameters, switching structures with up to three singular subarcs, up to two boundary subarcs of the first-order angle of attack constraint, up to one boundary subarc and up to four touch points of the third-order altitude constraint, and finally up to five bang-bang subarcs. These multiple subarcs can be detected during the computations by means of homotopy techniques and by a scrutiny of the necessary sign conditions for certain Lagrange multipliers. Because of the exceptional accuracy which can be obtained by the multiple-shooting method, a competing direct method is unlikely to be able to produce solutions with such high resolution. Note that, in the vicinity of solutions of certain multipoint boundary-value problems which satisfy only the usual first- and second-order necessary conditions, there are candidate optimal solutions which, in addition, satisfy those sign conditions and therefore yield a better performance index.

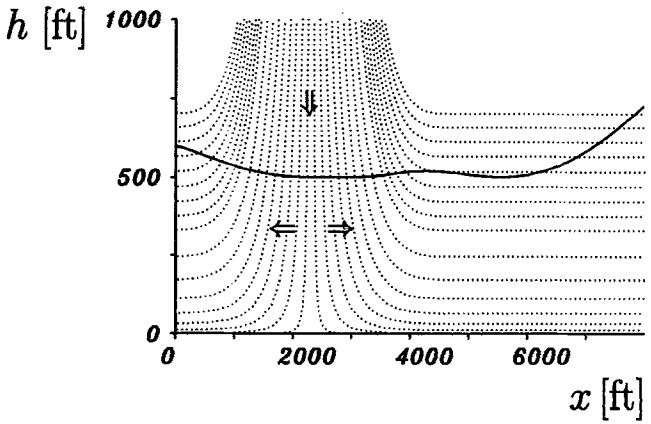

Fig. 28. Altitude over ground and wind profile for Wind Model 1; downburst: 50 ft/sec; shear: 100 ft/sec.

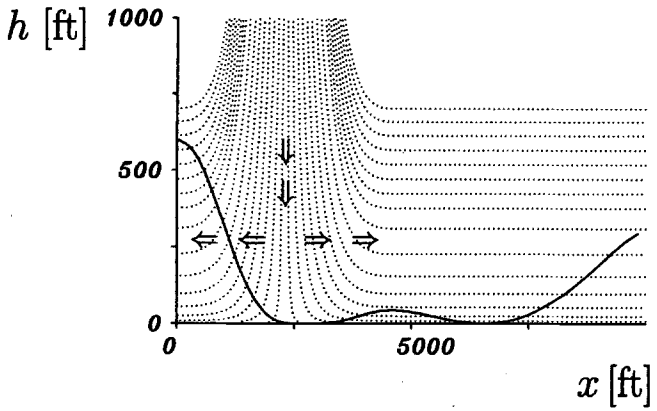

Fig. 29. Altitude over ground and wind profile for Wind Model 1; downburst: 100 ft/sec; shear: 200 ft/sec.

Although results of such an extremely high precision are not always needed, especially as the wind velocities are unpredictable, nevertheless the present approach provides an important tool for the computation and assessment of windshear recovering trajectories because of the combination of the best possible performance index, the outstanding accuracy of the multiple-shooting method, and the critical information provided by advanced necessary conditions of optimal control theory. This approach yields a high degree of assurance that the candidate optimal trajectories are really optimal. These

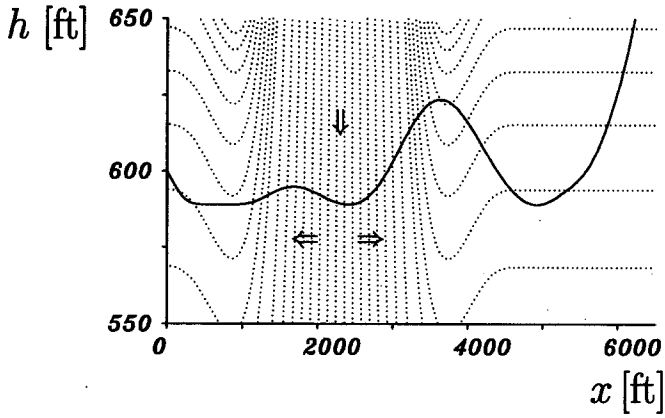

Fig. 30. Altitude over ground and wind profile for Wind Model 2; downburst: 50 ft/sec; shear: 100 ft/sec.

Table 6. Interior conditions for Wind Model 2 ($k=1$).

Switching points	t (sec)	Interior boundary conditions	Jump conditions
$t_{\text{bang},1}$	1.04	Eq. (15) [1]	
$t^s_{\text{entry},1}$	1.09	Eq. (18a) [1]	
$t^h_{\text{entry}} = t^s_{\text{exit},1}$	2.50	Eqs. (31a–d) [4][a,c]	Eqs. (32a)[c]
$t^s_{\text{entry},2} = t^h_{\text{exit}}$	4.42	Eq. (18a) [1]	
$t^s_{\text{exit},2}$	11.42	Eq. (18b) [1]	
$t^h_{\text{touch},1}$	11.53	Eqs. (27) [2][a]	Eq. (28a)
$t^s_{\text{entry},3}$	11.87	Eq. (18a) [1]	
$t^a_{\text{entry},1} = t^s_{\text{exit},3}$	13.80	Eqs. (24a, b) [2][b]	Eq. (22)[b]
$t^h_{\text{touch},2} = t^a_{\text{exit},1}$	23.05	Eqs. (27) [2][a,d]	Eq. (28a)
$t_{\text{bang},2}$	24.54	Eq. (15) [1]	
$t^a_{\text{entry},2}$	26.03	Eqs. (24a, b) [2][b]	Eq. (22)[b]

[a] If $\tilde{\zeta}$ is to be used as parameter, Eqs. (27a) and (31a) have to be replaced by Eqs. (37b).

[b] If $\sigma_0^{(1)}$ and $\sigma_0^{(2)}$ [for two subarcs due to the constraint (9)] are to be eliminated, Eq. (22) has to be replaced by Eq. (38). In this case, Eq. (24b) must be cancelled and the integration must be performed in a backward manner.

[c] Here, $\bar{\sigma}_2$ can be eliminated from the fifth component of Eq. (32a). For that, Eq. (31d) has to be cancelled and the fifth component of Eq. (32a) has to be replaced by (39). In the other components of Eq. (32a), $\bar{\sigma}_2$ has to be substituted. The integration must also be performed backward here.

[d] Here, the transversality conditions for the terminal time and the terminal flight path angle, both unspecified, are additionally satisfied. Equation (24c) is also satisfied.

optimal trajectories may then serve as benchmark trajectories both for guidance schemes and also for numerical methods for problems of optimal control.

References

1. LONG, M. E., *The Air-Safety Challenge*, National Geographic, Vol. 152, No. 2, pp. 209–235, 1977.
2. MIELE, A., WANG, T., TZENG, C. Y., and MELVIN, W. W., *Optimal Abort Landing Trajectories in the Presence of Windshear*, Journal of Optimization Theory and Applications, Vol. 55, No. 2, pp. 165–202, 1987.
3. GRANTHAM, W. J., and PARKS, E. K., *A DFW Microburst Model Based on DL-191 Data*, Proceedings of the 29th IEEE Conference on Decision and Control, Honolulu, Hawaii, Vol. 2, pp. 695–701, 1990.
4. MIELE, A., WANG, T., and MELVIN, W. W., *Optimal Take-Off Trajectories in the Presence of Windshear*, Journal of Optimization Theory and Applications, Vol. 49, No. 1, pp. 1–45, 1986.
5. MIELE, A., WANG, T., and MELVIN, W. W., *Guidance Strategies for Near-Optimum Take-Off Performance in a Windshear*, Journal of Optimization Theory and Applications, Vol. 50, No. 1, pp. 1–47, 1986.
6. MIELE, A., WANG, T., MELVIN, W. W., and BOWLES, R. L., *Maximum Survival Capability of an Aircraft in a Severe Windshear*, Journal of Optimization Theory and Applications, Vol. 53, No. 2, pp. 181–217, 1987.
7. MIELE, A., WANG, T., and MELVIN, W. W., *Quasi-Steady Flight to Quasi-Steady Flight Transition in a Windshear: Trajectory Optimization and Guidance*, Journal of Optimization Theory and Applications, Vol. 54, No. 2, pp. 203–240, 1987.
8. MIELE, A., WANG, T., and MELVIN, W. W., *Optimization and Acceleration Guidance of Flight Trajectories in a Windshear*, Journal of Guidance, Control, and Dynamics, Vol. 10, No. 4, pp. 368–377, 1987.
9. MIELE, A., WANG, T., WANG, H., and MELVIN, W. W., *Optimal Penetration Landing Trajectories in the Presence of Windshear*, Journal of Optimization Theory and Applications, Vol. 57, No. 1, pp. 1–40, 1988.
10. MIELE, A., WANG, T., MELVIN, W. W., and BOWLES, R. L., *Gamma Guidance Schemes for Flight in a Windshear*, Journal of Guidance, Control, and Dynamics, Vol. 11, No. 4, pp. 320–327, 1988.
11. MIELE, A., WANG, T., and MELVIN, W. W., *Quasi-Steady Flight to Quasi-Steady Flight Transition for Abort Landing in a Windshear: Trajectory Optimization and Guidance*, Journal of Optimization Theory and Applications, Vol. 58, No. 2, pp. 165–207, 1988.
12. MIELE, A., WANG, T., TZENG, C. Y., and MELVIN, W. W., *Abort Landing Guidance Trajectories in the Presence of Windshear*, Journal of the Franklin Institute, Vol. 326, No. 2, pp. 185–220, 1989.

13. MIELE, A., WANG, T., and MELVIN, W. W., *Penetration Landing Guidance Trajectories in the Presence of Windshear*, Journal of Guidance, Control, and Dynamics, Vol. 12, No. 6, pp. 806–814, 1989.
14. MIELE, A., WANG, T., MELVIN, W. W., and BOWLES, R. L., *Acceleration, Gamma, and Theta Guidance for Abort Landing in a Windshear*, Journal of Guidance, Control, and Dynamics, Vol. 12, No. 6, pp. 815–821, 1989.
15. MIELE, A., *Final Report on NASA Grant No. NAG-1-156: Optimization and Guidance of Flight Trajectories in the Presence of Windshear, 1984–1989*, Aero-Astronautics Report No. 244, Rice University, Houston, Texas, 1989.
16. MIELE, A., WANG, T., WANG, H., and MELVIN, W. W., *Overview of Optimal Trajectories for Flight in Windshear*, Control and Dynamic Systems, Edited by C. T. Leondes, Academic Press, New York, New York, Vol. 34, pp. 81–124, 1990.
17. MIELE, A., WANG, T., and MELVIN, W. W., *Wind Identification along a Flight Trajectory, Part 1: 3D-Kinematic Approach*, Journal of Optimization Theory and Applications, Vol. 75, No. 1, pp. 1–31, 1992.
18. MIELE, A., WANG, T., and MELVIN, W. W., *Wind Identification along a Flight Trajectory, Part 2: 2D-Kinematic Approach*, Journal of Optimization Theory and Applications, Vol. 76, No. 1, pp. 33–55, 1993.
19. MIELE, A., WANG, T., and MELVIN, W. W., *Wind Identification along a Flight Trajectory, Part 3: 2D-Dynamic Approach*, Journal of Optimization Theory and Applications, Vol. 77, No. 1, pp. 1–29, 1993.
20. BRYSON, A. E., JR., and ZHAO, Y., *Feedback Control for Penetrating a Downburst*, AIAA Paper No. AIAA-87-2343, 1987.
21. ZHAO, Y., and BRYSON, A. E., JR., *Optimal Paths through Downbursts*, Journal of Guidance, Control, and Dynamics, Vol. 13, No. 5, pp. 813–818, 1990.
22. ZHAO, Y., and BRYSON, A. E., JR., *Control of an Aircraft in Downbursts*, Journal of Guidance, Control, and Dynamics, Vol. 13, No. 5, pp. 819–823, 1990.
23. ZHAO, Y., and BRYSON, A. E., JR., *Aircraft Control in a Downburst on Takeoff and Landing*, Proceedings of the 29th IEEE Conference on Decision and Control, Honolulu, Hawaii, Vol. 2, pp. 753–756, 1990.
24. ZHAO, Y., and BRYSON, A. E., JR., *Approach Guidance in a Downburst*, Journal of Guidance, Control, and Dynamics, Vol. 15, No. 4, pp. 893–900, 1992.
25. LEITMANN, G., and PANDEY, S., *Aircraft Control under Conditions of Windshear*, Control and Dynamic Systems, Edited by C. T. Leondes, Academic Press, New York, New York, Vol. 34, pp. 1–79, 1990.
26. KAITALA, V., LEITMANN, G., and PANDEY, S., *Robust Aircraft Take-Off Control: A Comparison of Aircraft Performance under Different Windshear Conditions*, Differential Games—Developments in Modelling and Computation, Edited by R. P. Hämäläinen and H. K. Ehtamo, Springer, Berlin, Germany, pp. 235–244, 1991.
27. LEITMANN, G., and PANDEY, S., *Aircraft Control for Flight in an Uncertain Environment: Takeoff in Windshear*, Journal of Optimization Theory and Applications, Vol. 70, No. 1, pp. 25–55, 1991.
28. BOTKIN, N. D., KLEIN, V. M., PATSKO, V. S., and TUROVA, V. L., *Aircraft Landing Control in the Presence of Windshear*, Problems of Control and Information Theory, Vol. 18, No. 4, pp. 223–235, 1989.

29. BOTKIN, N. D., ZARKH, M. A., and PATSKO, V. S., *Numerical Solution of a Linear Differential Game*, Differential Games—Developments in Modelling and Computation, Edited by R. P. Hämäläinen and H. K. Ehtamo, Springer, Berlin, Germany, pp. 226–234, 1991.
30. BULIRSCH, R., MONTRONE, F., and PESCH, H. J., *Abort Landing in the Presence of a Windshear as a Minimax Optimal Control Problem, Part 1: Necessary Conditions*, Journal of Optimization Theory and Applications, Vol. 70, No. 1, pp. 1–23, 1991.
31. BULIRSCH, R., MONTRONE, F., and PESCH, H. J., *Abort Landing in the Presence of a Windshear as a Minimax Optimal Control Problem, Part 2: Multiple Shooting and Homotopy*, Journal of Optimization Theory and Applications, Vol. 70, No. 2, pp. 223–254, 1991.
32. VISSER, H. G., *Optimal Lateral Escape Maneuvers for Microburst Encounters during Final Approach*, Report LR-691, Faculty of Aerospace Engineering, Delft University of Technology, Delft, Netherlands, 1992.
33. BULIRSCH, R., *Die Mehrzielmethode zur numerischen Lösung von nichtlinearen Randwertproblemen und Aufgaben der optimalen Steuerung*, Report of the Carl-Cranz Gesellschaft, DLR, Oberpfaffenhofen, Germany, 1971.
34. STOER, J., and BULIRSCH, R., *Introduction to Numerical Analysis*, Springer, New York, New York, 1993.
35. DEUFLHARD, P., *A Modified Newton Method for the Solution of Ill-Conditioned Systems of Nonlinear Equations with Application to Multiple Shooting*, Numerische Mathematik, Vol. 22, pp. 289–315, 1974.
36. DEUFLHARD, P., *A Relaxation Strategy for the Modified Newton Method*, Optimization and Optimal Control, Edited by R. Bulirsch *et al.*, Springer, Berlin, Germany, pp. 59–73, 1975.
37. OBERLE, H. J., *Numerische Berechnung optimaler Steuerungen von Heizung und Kühlung für ein realistisches Sonnenhausmodell*, Habilitationsschrift, Munich University of Technology, Munich, Germany, 1982.
38. MAURER, H., *Optimale Steuerprozesse mit Zustandsbeschränkungen*, Habilitationsschrift, University of Würzburg, Würzburg, Germany, 1976.
39. BOWLES, R. L., *Windshear Detection and Avoidance: Airborne Systems Survey*, Proceedings of the 29th IEEE Conference on Decision and Control, Honolulu, Hawaii, Vol. 2, pp. 708–736, 1990.
40. BRYSON, A. E., JR., and HO, Y. C., *Applied Optimal Control*, Ginn and Company, Waltham, Massachusetts, 1969.
41. PESCH, H. J., *Offline and Online Computation of Optimal Trajectories in the Aerospace Field*, Applied Mathematics in Aerospace Science and Engineering, Edited by A. Miele and A. Salvetti, Plenum Publishing Corporation, New York, New York, pp. 165–219, 1994.
42. MCDANELL, J. P., and POWERS, W. F., *Necessary Conditions for Joining Optimal Singular and Nonsingular Subarcs*, SIAM Journal on Control, Vol. 9, pp. 161–173, 1971.
43. KELLEY, H. J., KOPP, R. E., and MOYER, H. G., *Singular Extremals*, Topics in Optimization, Edited by G. Leitmann, Academic Press, New York, New York, pp. 63–101, 1967.

44. OBERLE, H. J., and GRIMM, W., *BNDSCO—A Program for the Numerical Solution of Optimal Control Problems*, Internal Report No. 515-89/22, Institute for Flight Systems Dynamics, DLR, Oberpfaffenhofen, Germany, 1989.
45. HARTL, R. F., SETHI, S. P., and VICKSON, R. G., *A Survey of the Maximum Principles for Optimal Control Problems with State Constraints*, Research Report No 153, Institute for Econometrics, Operations Research, and System Theory, Vienna University of Technology, Vienna, Austria, 1992.
46. WOLFSON, M., ET AL., *Characteristics of Thunderstorm-Generated Low Altitude Wind Shear: A Survey Based on Nationwide Terminal Doppler Weather Radar Testbed Measurements*, Proceedings of the 29th IEEE Conference on Decision and Control, Honolulu, Hawaii, Vol. 2, pp. 682–688, 1990.